

# SOLAR SAIL ATTITUDE DYNAMICS AND CONING CONTROL TO ATTAIN DESIRED ORBITAL EFFECTS

Farheen Rizvi<sup>(1)</sup>, and Dale Lawrence<sup>(2)</sup>

<sup>(1)</sup>University of Colorado-Boulder, Aerospace Engineering Sciences Department, University of Colorado 429 UCB, Boulder, CO, 80309, 818-354-1324, farheen.rizvi@jpl.nasa.gov

<sup>(2)</sup>University of Colorado-Boulder, Aerospace Engineering Sciences Department, University of Colorado 429 UCB, Boulder, CO, 80309, 303-492-3025, dale.lawrence@colorado.edu

**Abstract:** A control method is developed for the solar sail normal vector to trace a desired circular coning trajectory at orbit rate. The coning trajectory is defined in the local vertical local horizontal (LVLH) frame and the coning occurs about an LVLH equilibrium sail attitude. Past research has shown that sail attitude equilibria exist in the LVLH frame under the influence of aerodynamic, gravity gradient and solar torques. Precession of the sail normal from these equilibria causes sail normal coning about that equilibrium attitude. If the coning happens at orbit rate, wide variety of orbital effects can be induced. This results in an inexpensive spacecraft with a longer duration mission as compared to other conventional efforts. A special case of analyzing circular cones (at orbit rate coning) reveals that desired orbital effects are induced by employing the sail coning method. The control method herein minimizes the angular momentum error between the actual and desired angular momentum vectors at orbit rate. Since angular momentum is a function of sail normal, angular momentum error reduction raises hope in reducing the sail normal error between the actual and desired sail normal vectors as well. Results for tracking a  $1^\circ$  circular cone about an LVLH equilibrium point where maximum orbital effects are induced is presented. The sail normal is traced with an accuracy of  $0.05^\circ$ . The control torques required to induce this circular orbit rate coning are on the order of  $10^{-6}$  Nm (acceptable on small sailcraft).

---

<sup>1</sup> Farheen Rizvi is now with Jet Propulsion Lab (NASA-CALTECH), contact: M.S. 230-104, 4800 Oak Grove Drive, Pasadena, CA, 91109, 818-354-1324

<sup>2</sup> Dr. Dale Lawrence has served as an adviser throughout this work

**Keywords:** solar sail normal, circular orbit rate coning, LVLH attitude equilibria, angular momentum error reduction, desired orbital effects

## 1. Introduction

Solar sails are an attractive solution for expensive and massive space missions. Traditional spacecraft must carry in-space propulsion fuel that increases both launch mass and cost. A sail exposed to solar radiation offers free and continuous propulsion by manipulating the sail thrust vector direction relative to the Sun. Figure 1 illustrates a simple solar sail configuration and Fig. 2 shows how the solar radiation thrust force is used for propulsion.

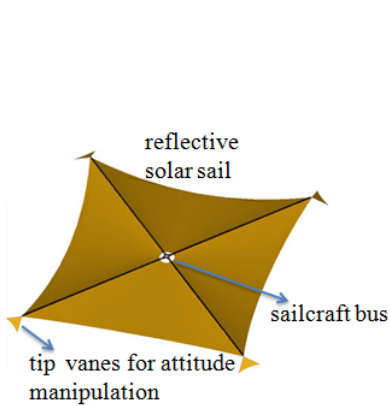


**Figure 1. Solar sail configuration**

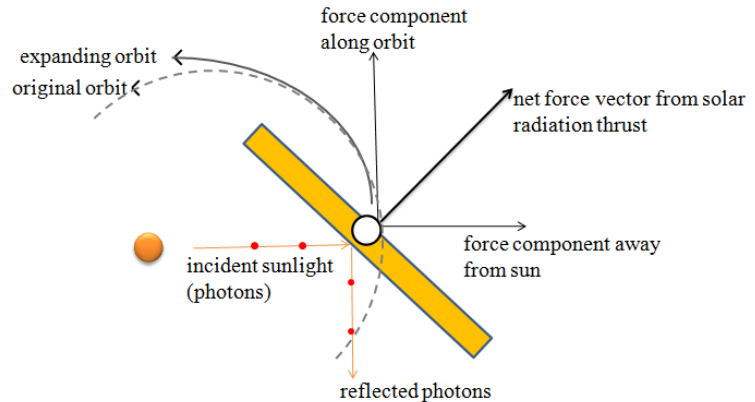
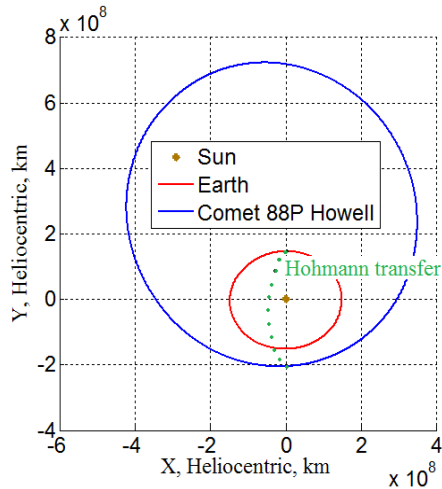


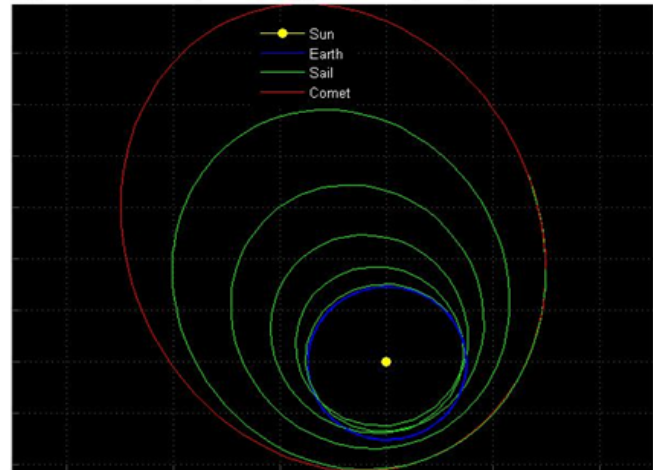
**Figure 2. Solar radiation thrust force**

A solar sail consists of a sailcraft bus that houses the necessary electronics and hardware, a large, reflective, gossamer sail and an attitude manipulation component (tip vanes, thrusters, reaction wheels). The integrated effect of the reflected photons provides the propulsive thrust force. A large sail area is required in order to interrupt the photon radiation and produce an appreciable amount of thrust force. Since acceleration is inversely proportional to mass for a given thrust force, the mass of the sailcraft must be kept to a minimum. Thus, the sail and bus are designed to provide a large area-to-mass ratio and maximize the propulsion acceleration. Incident rays of sunlight reflect off of the sail (assume specular reflection from a perfectly flat sail) and produce two force components: one in the direction of the incident sunlight and another in the opposite direction of the reflected rays. In the net force vector, the components tangent to the sail surface cancel and the components normal to the surface add to produce the thrust force approximately in the sail normal direction. NASA's CubeSail project used a perfectly reflective  $40 \text{ m}^2$  square sail in simulation to show that at 1 AU from the Sun, 0.03 N of solar radiation thrust force can be produced [1]. Although this force is relatively small compared with other propulsion methods, it is available continuously and hence can still be used to propel spacecraft for long distances without carrying any propellant.

The free propulsion from solar radiation makes extended mission durations feasible with reduced spacecraft mass and cost. A typical science mission is expected to cost on the order of one million dollars per kilogram of spacecraft mass [1]. This leaves high potential for low-cost science missions that have reduced spacecraft mass. As an example, results from a comet rendezvous mission study to reach Comet 88P/Howell using chemical propulsion and solar sailing are shown in Figure 3.



[Rizvi, et. al. 2009]



[Stough, et. al. 2008]

**Figure 3. Comet Rendezvous Mission Study Using Chemical and Solar Sail Propulsion**

Via traditional chemical propulsion, a Hohmann transfer from the Earth to the comet required 400 kg of propellant mass, whereas the solar sail completed the same mission with a total spacecraft mass of 3 kg (a factor of ~135 reduction in spacecraft mass). This translates into lower launch costs to Earth escape velocity and reduced development costs for the spacecraft [2]. The transfer time for the high thrust approach using chemical propulsion was 0.7 years as compared with 10 years for the solar sail. Therefore, for missions where transfer time is not a critical parameter, solar sail propulsion can result in significant fuel mass savings.

The significant solar thrust propulsion enables non-Keplerian orbits for solar sails. With this unique capability of solar sails, many space science missions can be achieved which are difficult to implement using conventional (chemical) propulsion techniques. Conventional propulsion can only produce Keplerian orbits such as ellipses, parabola and hyperbola (parts of a conic section). However, non-Keplerian orbits can be produced with constant sail thrusting through which orbit raising and precession can be achieved. One such mission is the study of the Earth magnetotail for which non-Keplerian orbits are desired. This requires the spacecraft orbit to continuously rotate to follow a Sun-synchronous path and also raise its orbit to explore the entire magnetotail. Two mission scenarios using conventional and solar sail propulsion are illustrated in Figure 4.

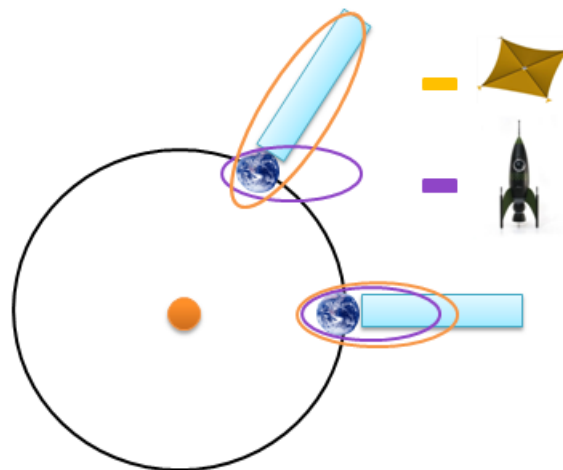


**Figure 4. Exploring Earth Magnetotail Using Chemical and Solar Sail Propulsion**

The chemical propulsion (purple line – rocket) with fuel enough for initial orbit injection produces an elliptical orbit, which then stays inertially fixed as the Earth (along with the magnetotail) rotates about the Sun. Since the magnetotail rotates with the Sun-Earth line, an inertially fixed Keplerian orbit with spacecraft apogee inside the magnetotail provides less than three months of science data. The spacecraft collects data for a limited time until the magnetotail rotates away with the Earth. In contrast, the solar sail propulsion system provides a unique steering capability that enables long-term residence within the magnetotail. In addition, the sail orbit can also be raised to provide full coverage of the magnetotail. The solar sail propulsion (yellow line – sail) allows the semi-major axis of the orbit to increase and precess with the Earth rotation. With a continuous Sun-synchronous apse-line precession to rotate and raise an elliptical Earth orbit, at least two years of scientific data could be returned [3]. Solar sail propulsion may provide an optimum propulsion system over conventional chemical propulsion, at least in some missions. It may also have advantages over electric propulsion due to the ease in attaining non-Keplerian orbits with reduced mission mass and cost [4].

### **1.1 Solar Sail Attitude Dynamics and Control**

Solar sail research on orbit analysis focuses on producing orbit raising/lowering and inducing orbital effects using the sails. These effects can yield otherwise expensive orbits such as Sun-synchronous and halo types. Orbit changes result from orienting the thrust vector, and in order to achieve the desired orbital effects, the sail must operate at the required attitude to modulate the solar thrust. Thus, orbit analysis has also motivated the research work on sail attitude manipulation. Sails typically contain a small spacecraft bus in the midst of a large, gossamer structure. Most sail work has addressed feasibility concerns related to orbit analysis and structural sail dynamics. Due to this configuration, significant solar, aerodynamic and gravity gradient torques act on the sail and can disturb the sail orientation (attitude) relative to the sun. Accordingly, large control torques are needed to counteract these attitude disturbances, and an understanding of sail attitude dynamics is required in order to design appropriate control algorithms.

Recent studies have analyzed natural sail dynamics in order to maintain the desired thrust vector pointing [5 and 6]. Generally, large external torques are required to maintain the desired thrust vector pointing relative to the Sun. Lawrence, et. al. have shown that specific kinds of torques can be generated naturally under the influence of solar, aerodynamic and gravity gradient torques [5]. This reduces the need for expensive and massive traditional attitude control techniques (attitude jets or reaction wheels). The basic idea is to operate at the attitude equilibria of the sail normal vector in the local vertical local horizontal (LVLH) frame. An extension of this idea is to utilize a slight deviation of the sail normal from these equilibria, which results in sail normal coning about that equilibrium. McMahan, et. al. have shown that any desired orbit changes can be obtained with sail normal coning at orbit rate (circular cones) [6].

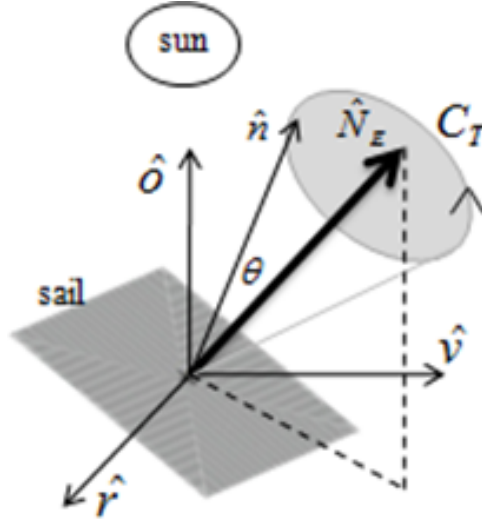


**Figure 5. Solar Normal Coning in Local Vertical Local Horizontal Frame**

In Fig. 5, the sail normal cones about the LVLH equilibrium attitude,  $\hat{N}_E$ . With a slight deviation,  $\theta$  from the equilibrium attitude, the normal vector,  $\hat{n}$  traces a coning trajectory,  $C_T$  in the L-frame (defines natural sail coning). The cone tracing should occur at orbit rate to attain desired sail orbit changes. Swartwout, et. al.'s sail steering law also produces the desired orbital effects, however with significant control torque and rapid maneuvers that can damage the sail [7]. In contrast, McMahon's approach produces smooth sail rotation rates that avoid disturbing the structural sail dynamics [6]. In his work, all ranges of the desired orbital effects can be attained when the natural sail coning occurs at orbit rate [6]. This work intends to build upon these studies and explore the feasibility of designing a control that can enable the sail normal to trace a circular coning trajectory at orbit rate.

## 2. Solar Sail Coning Dynamics

In this section, the dynamics of the solar sail are presented. With the sail dynamics, the concept of sail attitude equilibrium in the local vertical local horizontal frame (L-frame) is explained. The L-frame sail attitude equilibria enable sail normal coning in the inertial frame (A-frame). A small perturbation from the sail attitude equilibria induces L-frame coning of the sail normal about those sail equilibria. This L-frame coning of the sail is discussed. Natural environmental torques can cause sail precession and enable L-frame sail coning.

Many orbital effects can be obtained due to the L-frame coning of the sail normal about the sail equilibria. However, the natural rate and shape of coning of the sail normal about the sail equilibrium point does not yield the desired orbital effects. Control torques can be used to enforce the desired rate and coning shape (circular cones). Results showing the coning of the sail normal in the L-frame about the sail equilibrium are presented.

### 2.1. Reference Frames

In order to describe the sail dynamics in a circular orbit, the reference frames used are given in Figure 6 [5].

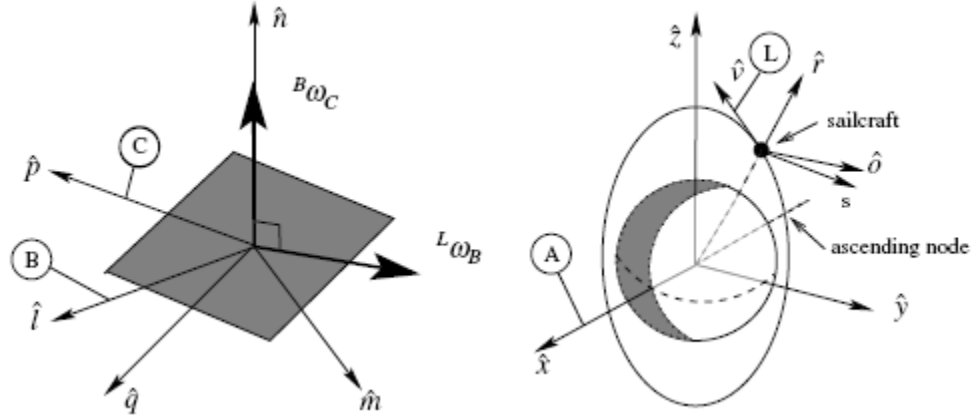


**Figure 6. Reference Frames used to Develop Sail Dynamics<sup>5</sup>**

The A-frame  $\{\hat{x}, \hat{y}, \hat{z}\}$  is the inertial (fixed) frame. The  $\hat{x}$  and  $\hat{y}$  define the Earth equatorial frame with  $\hat{x}$  pointing along the vernal equinox. The  $\hat{z}$  is normal to the equatorial frame. The local vertical local horizontal or L-frame  $\{\hat{r}, \hat{v}, \hat{o}\}$  rotates along with the orbit at orbit rate. The  $\hat{r}$  points along the orbit radial direction,  $\hat{v}$  is in the direction of the sail velocity vector and  $\hat{o}$  is aligned with the orbit angular momentum. The C-frame  $\{\hat{n}, \hat{p}, \hat{q}\}$  is the sail body-fixed frame. The  $\hat{n}$  points along the sail normal vector (normal to the plane of the sail). The  $\hat{p}$  and  $\hat{q}$  remain in the plane of the sail. The B-frame  $\{\hat{n}, \hat{l}, \hat{m}\}$  is also a body frame except that it does not rotate with the sail in the rotation about  $\hat{n}$ . The  $\hat{l}$  and  $\hat{m}$  lie in the plane of the sail. Thus, the only difference between the B-frame and C-frame is the rotation about  $\hat{n}$ . The B-frame is taken to be aligned with the C-frame at the initial time epoch.

## 2.2. Description of Sail Equilibria in L-frame and Inertial Sail Normal Coning

Any fixed sail normal  $\hat{n}$  in the L-frame describes the sail equilibrium attitude in the L-frame. The sail attitude can be defined by the sail normal vector,  $\hat{n}$  because the sail is symmetric about  $\hat{n}$  and the rotation about  $\hat{n}$  does not alter the forces on the sail. When the sail normal,  $\hat{n}$  is fixed in the L-frame, but not aligned with  $\hat{o}$ , the sail rotates with the orbit and produces inertial coning of  $\hat{n}$  at orbit rate.

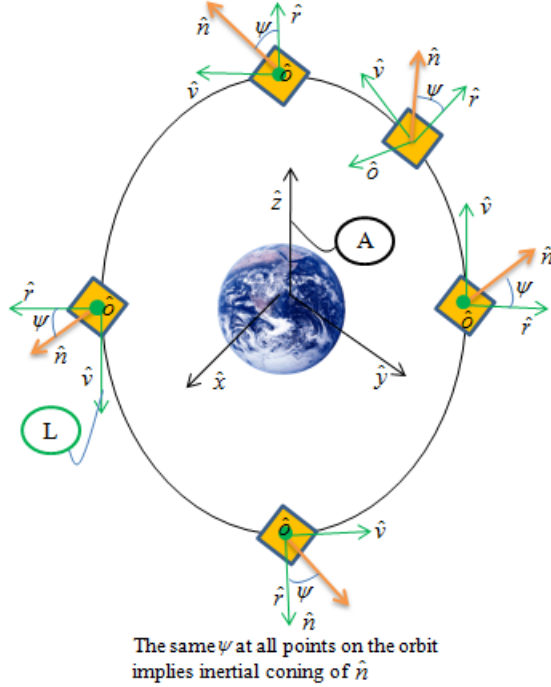


**Figure 7. Illustration of Inertial Coning of the L-frame Fixed Sail Normal**

In Figure 7, the sail normal remains fixed in the L-frame (indicated by the constant angle  $\psi$ ) and causes inertial coning of  $\hat{n}$  at orbit rate. By choosing  $\psi$  appropriately, the sail angular momentum precesses to provide inertial coning with desirable orbit change effects. The angular momentum precession, in turn, is caused by torques acting on the sail. For  $\hat{n}$  to remain fixed in the L-frame and enable inertial coning, the sail angular momentum must precess at a desired rate.

$${}^A \begin{bmatrix} \dot{\hat{h}}_{desired} \end{bmatrix} = \tau_{required} \quad (1)$$

where  $\dot{\hat{h}}_{desired}$  and  $\tau_{required}$  are the desired precession of the angular momentum and required torque to attain this desired motion, respectively. Lawrence, et. al. [6] have shown that this  $\tau_{required}$  can be achieved with naturally induced environmental torques (atmospheric, gravity gradient and solar) acting on the sail.

### 2.3. L-frame Sail Normal Coning

The sail normal  $\hat{n}$  can be described in the L-frame via a cone angle  $\beta$  and a clock angle  $\phi$ .

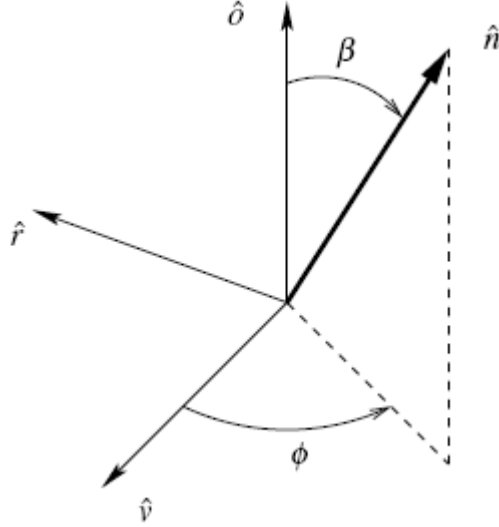


**Figure 8. Cone and Clock Angles of the Sail Normal relative to the L-frame<sup>5</sup>**

From Figure 8 [5], the sail normal,  $\hat{n}$  becomes

$$\hat{n} = -(\sin \beta \sin \phi)\hat{r} + (\sin \beta \cos \phi)\hat{v} + (\cos \beta)\hat{o} \quad (2)$$

Lawrence, et. al. have shown that for the developed sail dynamics, a small sail normal perturbation from the L-frame attitude equilibrium enables the sail normal to cone about that equilibrium point [5]. This constitutes sail normal coning in the L-frame illustrated in Figure 9.

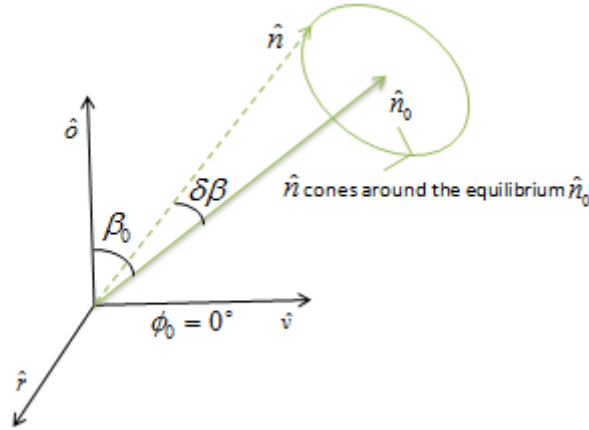


**Figure 9. Illustration of the Sail Normal Coning in the L-frame**

The  $\hat{n}_0$  exhibits the sail equilibrium point and  $\hat{n}$  is the coning sail normal vector. The perturbation is given by a small deviation,  $\delta\beta$  in the cone angle,  $\beta$ . The coning is defined such that the cone need not be circular or have a fixed coning rate. McMahan, et. al. have shown that desired orbital effects can be induced when the L-frame coning occurs at orbit rate such that one rotation of  $\hat{n}$  around  $\hat{n}_0$  is completed in one orbital period and has a circular coning shape [6]. They state that the greatest orbital effects can be induced when the sail normal is operated at  $\beta = 35^\circ$  and  $\phi = 0^\circ$  for  $1^\circ$  cones. This study is performed using these parameters.

## 2.4. Natural Dynamics of Sail Normal Coning in L-frame using CubeSail Simulation

Lawrence, et. al. have created a MATLAB simulation for a CubeSail (small solar sail satellite) that propagates the sailcraft attitude under the influence of aerodynamic, solar pressure and gravity gradient torques over a circular, Low Earth Orbit [5]. The sailcraft studied consists of a solar sail and sailcraft bus, which is located out of the sail plane. The sailcraft model used in this study is shown in Figure 10.

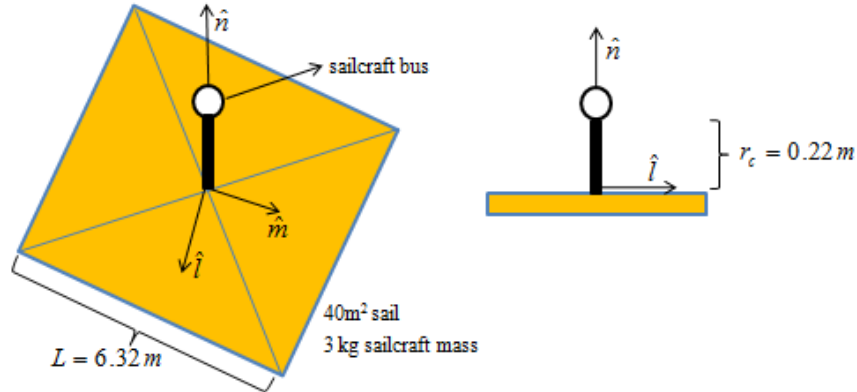


**Figure 10. Physical Components and Dimensions of the Sailcraft Model**

The sail is assumed to be flat, rigid, uniform, square with a sailcraft bus located out of the sail plane at a distance  $r_c$  along the sail normal,  $\hat{n}$ . Since the sail is symmetric and rotation about  $\hat{n}$  does not alter any solar, aerodynamic, or gravity gradient forces, the sail attitude can be described only by the sail normal vector when considering these external effects. The bus is located near the plane of the sail (0.22 m) as compared with the sail size ( $40 \text{ m}^2$ ), which enables the sailcraft moment of inertia to be similar to that of a flat plate [8]. A large, gossamer sail will be non-rigid in space. It is argued that the orbital element control applications using coning motions produce smooth, low frequency environmental torques, on the order of orbit frequency and require closed loop settling times on the order of several orbits. The disturbance frequencies and control system bandwidths are on the order of  $10^{-4}$  Hz (for 700 km Low Earth Orbit), whereas the lowest structural modes of the sail are in the range of  $10^{-1}$  to  $10^{-2}$  Hz [4]. This suggests that the torque applications do not excite the sail structural modes, thus justifying the rigid body assumption from a control-structure interaction viewpoint. Non-uniform material properties within the sail will cause imperfect solar reflections and variations in pressure-loading on the sail. The varying pressure-loading issue will deform the sail and hence it will no longer remain flat in orbit. A deformed sail will experience different torques as a function of attitude. However, the varying pressure-loading issue is a secondary effect and offers more insight on the sailcraft torque as a function of attitude by deviating from the ideal case. This study focuses on the ideal (flat) case. The case of a non-spinning sail is analyzed in this work. The orbit and sailcraft parameters used are shown in Table 1.

**Table 1. Orbit and Sailcraft Parameters**

<b>Orbit Parameters</b>	
Altitude, $a$	700 km
Inclination, $i$	90°
Right ascension of ascending node, $\Omega$	180°
Orbit rate, $\omega_o$	1.06 x 10 <sup>-3</sup> rad/s
Right ascension of sun, $r_s$	90°
Declination of sun, $d_s$	0°
Solar flux at 1 AU, $F_s$	1358 W/m <sup>2</sup>
Atmospheric density, $\rho$	5 x 10 <sup>-14</sup> kg/m <sup>3</sup>
Aerodynamic moment coefficient, $\tau_{am}$	1.18 x 10 <sup>-5</sup> Nm
Solar moment coefficient, $\tau_{sm}$	9.84 x 10 <sup>-6</sup> Nm
Gravity gradient moment coefficient, $\tau_{gm}$	6.33 x 10 <sup>-6</sup> Nm
<b>Sailcraft Parameters</b>	
Sail side length, $L$	6.325 m
Sail mass, $m_s$	1.7 kg
Sailcraft bus mass, $m_b$	1.3 kg
Distance to bus from sail plane in $\hat{n}$ direction, $r_c$	0.22 m
Axial moment of inertia, $I_n$	11.3 kgm <sup>2</sup>
Transverse moment of inertia, $I_t$	5.7 kgm <sup>2</sup>
Sail reflectivity, $s$	0.9
Aerodynamic coefficient of drag, $C_d$	2.2
Specular reflectance fraction, $f_s$	0.7

The simulation is run for three orbital periods and shows the results for the motion of the sail normal,  $\hat{n}$  in the L-frame.

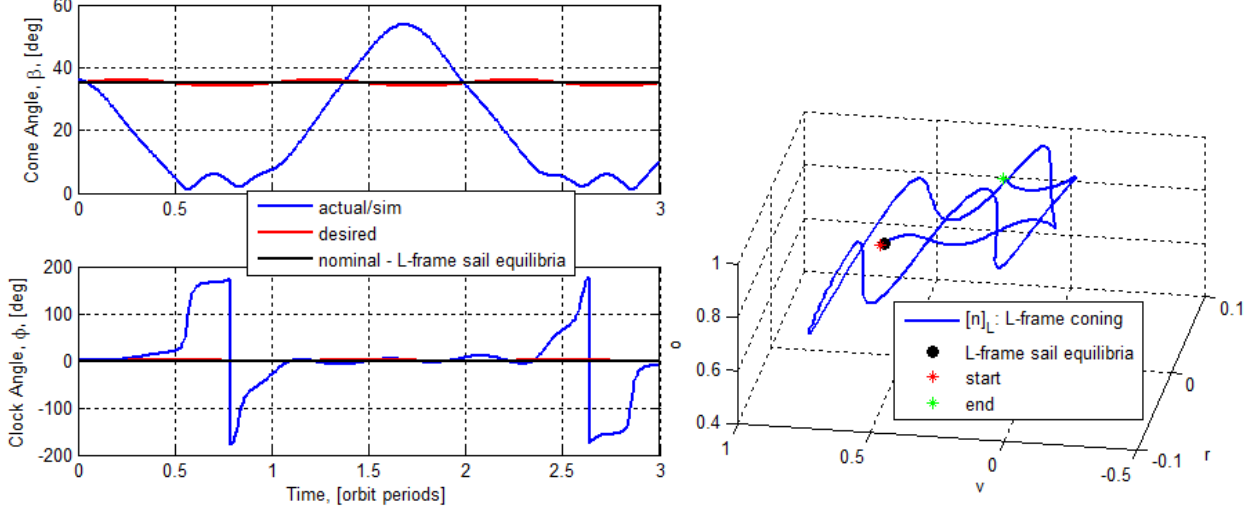


**Figure 11. Sail Normal Coning in the L-frame about the Equilibrium Point,  $[\beta=35^\circ, \phi=0^\circ]$**

The three-dimensional plot shows the motion of  $\hat{n}$  in the L-frame. The two-dimensional plot gives a time history of the cone and clock angles over the course of several orbital periods. The  $\hat{n}$  cones about the equilibrium point in the L-frame. However, the coning does not occur at orbit rate (one cone is traced in two orbits). In addition, the coning is not circular as  $\hat{n}$  moves in the vicinity of the equilibrium point.

Since the natural motion is not orbit rate circular coning (desired for useful orbital effects) control torques on the sailcraft are necessary. The control torque induces the desired coning and enforces orbit rate coning. The part of the control torque used to induce the desired coning (referred to as coning control torque) allows the sail normal to trace the desired shape of the coning trajectory, whereas the other part of the control torque enforcing orbit rate coning (called as the rate control torque) allows the sail normal to trace the trajectory at the desired rate. The total control torque required to attain the desired orbit rate circular coning is a combination of these two control torques. The next section addresses the type of control method that can be used in order to enforce orbit rate circular coning and analyzes its performance.

### 3. Control Method

A control method is developed to enable the sail normal  $\hat{n}$  to track the desired sail normal  $\hat{n}_c$  on the circular coning trajectory and provide orbit rate coning in the L-frame. The control law must establish a relationship between the control torque,  $\tau_{control}$  and sail motion  $\hat{n}$  relative to the desired  $\hat{n}_c$  that provides closed loop stability. Note that the sail angular momentum,  $\vec{h}$  and  $\tau_{control}$  are related by the simple dynamics  ${}^{inertial} \left[ \dot{\vec{h}} \right] = \tau$ . Thus, a control method is developed such that  $\vec{h}$  tracks the desired angular momentum,  $\vec{h}_c$  on the coning trajectory at orbit rate. The control law is used to reduce the error between  $\vec{h}$  and  $\vec{h}_c$ . Since sail angular momentum is a function of sail normal/angular position or sail attitude (Eq. 14), the control law is created with the hope that

error reduction in angular momentum and thus tracking the desired angular momentum at orbit rate will also lead to tracking the desired sail angular position at orbit rate (enable  $\hat{n}$  to track  $\hat{n}_c$ ).

This control method enables the sail angular momentum vector  $\vec{h}_s$  to trace the sail angular momentum vector on the desired circular coning trajectory  $\vec{h}_c$  at orbit rate. This in-turn can cause the sail normal vector,  $\hat{n}$  to trace the desired normal,  $\hat{n}_c$  and hence yield the desired circular coning at orbit rate. Here  $\vec{h}_s$  is the simplified notation for the angular momentum vector of the C-frame as seen by the A-frame (given as  ${}^A[\vec{h}_s]_C$ ). Likewise,  $\vec{h}_c$  is the simplified notation for the desired angular momentum vector of the C-frame as seen by the A-frame (given as  ${}^A[\vec{h}_c]_C$ ). In order to prescribe  $\vec{h}_c$  the kinematics of the coning trajectory are calculated. For a given  $\beta_0$  and  $\phi_0$ , the desired coning trajectory is illustrated in Figure 12.

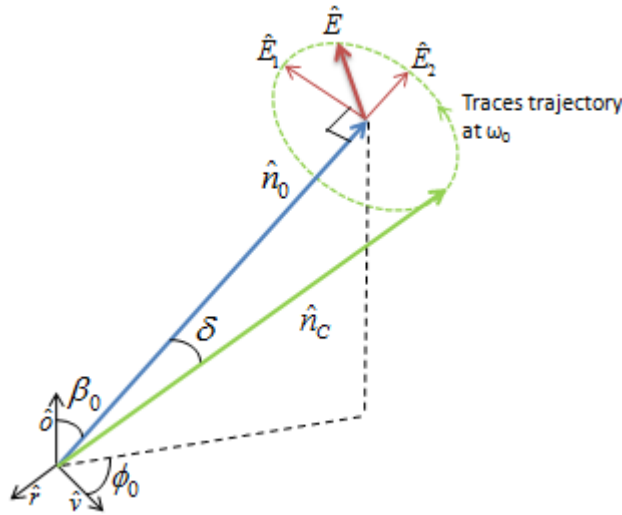


**Figure 12. Desired Coning Trajectory**

The desired trajectory traces a circular cone (half cone angle,  $\delta$ ) about nominal sail normal  $\hat{n}_0$  at orbit rate  $\omega_o$ . The cone lies in a plane perpendicular to  $\hat{n}_0$ . The sail normal position on the cone at each time step is given by  $\hat{n}_c$ . The motion of the sail normal  $\hat{n}_c$  is determined by rotating  $\hat{n}_0$  via a time-varying rotation matrix,  $R_c^0$  which has rotation axis  $\hat{E}$  and rotation angle  $\delta$ . In order to calculate  $\hat{E}$ , a vector,  $\hat{E}_1$  perpendicular to  $\hat{n}_0$  is defined in the L-frame components.

$$\hat{E}_1 \perp \hat{n}_0 \rightarrow [\hat{E}_1]_L = \begin{bmatrix} \cos(\beta_0) \cdot \sin(\phi_0) \\ -\cos(\beta_0) \cdot \cos(\phi_0) \\ \sin(\beta_0) \end{bmatrix} \quad (3)$$

A plane can be defined by two orthogonal vectors. Along with  $\hat{E}_1$ , the plane of the cone is determined by calculating another vector,  $\hat{E}_2 = \hat{E}_1 \times \hat{n}_0$ . Now, the vector  $\hat{E}$  at each time step can be expressed as a linear combination of  $\hat{E}_1$  and  $\hat{E}_2$  in the plane of the cone.

$$\hat{E} = \cos(\omega_0 t) \cdot \hat{E}_1 + \sin(\omega_0 t) \cdot \hat{E}_2 \quad (4)$$

With the rotation axis,  $\hat{E}$  and defined rotation angle,  $\delta$ , the rotation matrix,  $R_c^0$  is [9]

$$R_c^0 = \cos(\delta) \cdot I_{3 \times 3} + (1 - \cos \delta) \cdot \begin{bmatrix} \hat{E}(1)^2 & \hat{E}(1) \cdot \hat{E}(2) & \hat{E}(1) \cdot \hat{E}(3) \\ \hat{E}(1) \cdot \hat{E}(2) & \hat{E}(2)^2 & \hat{E}(2) \cdot \hat{E}(3) \\ \hat{E}(1) \cdot \hat{E}(3) & \hat{E}(2) \cdot \hat{E}(3) & \hat{E}(3)^2 \end{bmatrix} + \sin(\delta) \cdot \begin{bmatrix} 0 & \hat{E}(3) & -\hat{E}(2) \\ -\hat{E}(3) & 0 & \hat{E}(1) \\ \hat{E}(2) & -\hat{E}(1) & 0 \end{bmatrix} \quad (5)$$

and the sail normal,  $\hat{n}_c$  is given by  $\hat{n}_c = R_c^0 \cdot \hat{n}_0$ . Using the definition of the sail normal in the L-frame, the desired angular position ( $\beta_c$  and  $\phi_c$ ) of the sail at each time step on the coning trajectory can be computed as

$$[\hat{n}_c]_L = \begin{bmatrix} -\sin(\beta_c) \cdot \sin(\phi_c) \\ \sin(\beta_c) \cdot \cos(\phi_c) \\ \cos(\beta_c) \end{bmatrix} \Rightarrow \begin{cases} \beta_c = \cos^{-1}(\hat{n}_c(3)) \\ \phi_c = \tan^{-1}\left(\frac{-\hat{n}_c(1)}{\hat{n}_c(2)}\right) \end{cases} \quad (6)$$

Figure 13 presents an example of the desired circular coning trajectory (half cone angle,  $\delta = 1^\circ$ ) throughout one orbital period for a given sail equilibrium point at  $\beta_0 = 35^\circ$  and  $\phi_0 = 0^\circ$ .

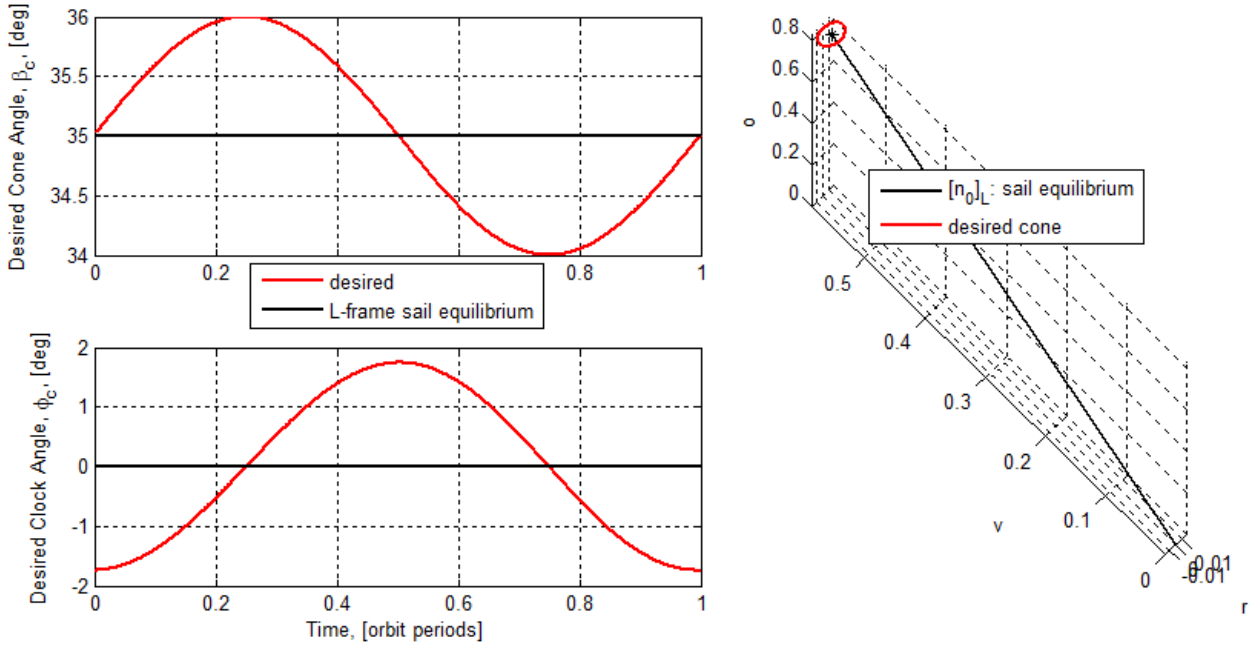


**Figure 13. Desired Circular Coning Trajectory having Half Cone Angle,  $\delta=1^\circ$  about a Nominal Sail Normal of  $\beta_0=35^\circ$ ,  $\Phi_0=0^\circ$  (One Orbital Period)**

The nominal sail normal  $\hat{n}_0$  is rotated at each time step with  $R_c^0$  to yield the desired cone given by  $\hat{n}_c$ . The  $\beta_c$  and  $\phi_c$  of the coning motion (extracted from  $\hat{n}_c$ ) exhibit sinusoidal behavior and can be expressed as

$$\begin{aligned}\beta_c &= \beta_0 + x \cdot \sin(\omega_0 \cdot t), x = \delta \\ \phi_c &= y \cdot \cos(\omega_0 \cdot t), y = \tan^{-1}\left(\frac{-\hat{n}_c(1)_{time=0}}{\hat{n}_c(2)_{time=0}}\right)\end{aligned}\quad (7)$$

From the desired angular position, the desired angular position rate ( $\dot{\beta}_c$  and  $\dot{\phi}_c$ ) is determined.

$$\begin{aligned}\dot{\beta}_c &= \delta \cdot \omega_0 \cdot \cos(\omega_0 \cdot t) \\ \dot{\phi}_c &= -y \cdot \omega_0 \cdot \sin(\omega_0 \cdot t), y = \tan^{-1}\left(\frac{-\hat{n}_c(1)_{time=0}}{\hat{n}_c(2)_{time=0}}\right)\end{aligned}\quad (8)$$

The rate also has sinusoidal motion. Along with the desired angular positions and rates, the desired angular velocity ( ${}^L\vec{\omega}_B^*$ ) is also required to derive the kinematics of the coning trajectory. The rate of change of  $\hat{n}_c$  in the L-frame is

$$\frac{{}^L d\hat{n}_c}{dt} = \frac{{}^B d\hat{n}_c}{dt} + {}^L\vec{\omega}_B \times \hat{n}_c \rightarrow \frac{d[\hat{n}_c]_L}{dt} = [{}^L\vec{\omega}_B]_L \times [\hat{n}_c]_L \quad (9)$$

since the sail normal is fixed in the B-frame. The B-frame is defined such that the motion of  $\hat{n}$  in the L-frame only describes the sail tip and tilt velocities (there is no rotation about the  $\hat{n}$  direction). Hence, Eq. 9 can define only two velocity components uniquely. Let the angular velocity components of  ${}^L\vec{\omega}_B$  in the L-frame be

$$[{}^L\vec{\omega}_B]_L = \begin{bmatrix} \omega_r \\ \omega_v \\ \omega_o \end{bmatrix}$$

Now  $\frac{d[\hat{n}_c]_L}{dt}$  can be expanded as

$$\frac{d[\hat{n}_c]_L}{dt} = \begin{bmatrix} -\sin \beta_c \cos \phi_c \dot{\phi}_c - \cos \beta_c \sin \phi_c \dot{\beta}_c \\ -\sin \beta_c \sin \phi_c \dot{\phi}_c + \cos \beta_c \cos \phi_c \dot{\beta}_c \\ -\sin \beta_c \dot{\beta}_c \end{bmatrix} = \begin{bmatrix} \omega_v \cos \beta_c - \omega_o \sin \beta_c \cos \phi_c \\ -\omega_r \cos \beta_c - \omega_o \sin \beta_c \sin \phi_c \\ \omega_r \sin \beta_c \cos \phi_c + \omega_v \sin \beta_c \sin \phi_c \end{bmatrix} \quad (10)$$

and re-arranged to give

$$\underbrace{\begin{bmatrix} 0 & \cos \beta_c & -\sin \beta_c \cos \phi_c \\ -\cos \beta_c & 0 & -\sin \beta_c \sin \phi_c \\ \sin \beta_c \cos \phi_c & \sin \beta_c \sin \phi_c & 0 \end{bmatrix}}_A \cdot \begin{bmatrix} \omega_r \\ \omega_v \\ \omega_o \end{bmatrix} = \begin{bmatrix} -\sin \beta_c \cos \phi_c \dot{\phi}_c - \cos \beta_c \sin \phi_c \dot{\beta}_c \\ -\sin \beta_c \sin \phi_c \dot{\phi}_c + \cos \beta_c \cos \phi_c \dot{\beta}_c \\ -\sin \beta_c \dot{\beta}_c \end{bmatrix} \quad (11)$$

The A matrix is singular because its determinant is found to be zero. One of the velocity components is linearly dependent on the other two and hence multiple solutions for  ${}^L\vec{\omega}_B$  exist. Figure 14 depicts the meaning of multiple solutions in this case.

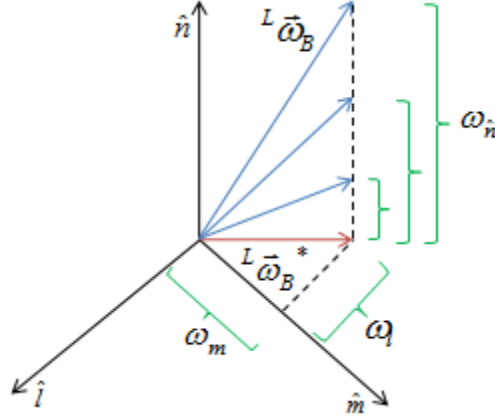


**Figure 14. Multiple Angular Velocity Solutions**

In Figure 14,  ${}^L\vec{\omega}_B$  is expressed in the B-frame components. All solutions have the same  $\hat{l}$  and  $\hat{m}$  components but different  $\hat{n}$  components because the use of  ${}^L\vec{\omega}_B \times \hat{n}_c$  equation makes the  $\hat{n}$  velocity component arbitrary (the kinematic Eq. 9 can only describe two velocity components uniquely). However, the B-frame is defined to have no component of the angular velocity in the  $\hat{n}$  direction. This requires the  $\hat{n}$  velocity component to be zero. Thus, the unique angular velocity solution,  ${}^L\vec{\omega}_B^*$  can be obtained by projecting one of the  ${}^L\vec{\omega}_B$  solutions onto the plane defined by  $\hat{n}_c$  such that no component of the angular velocity occurs in the sail normal direction.

$${}^L\vec{\omega}_B^* = (I_{3 \times 3} - \hat{n}_c \cdot \hat{n}_c) \cdot {}^L\vec{\omega}_B = {}^L\vec{\omega}_B - (\hat{n}_c \cdot {}^L\vec{\omega}_B) \hat{n}_c \quad (12)$$

The unique solution is obtained by removing any velocity component in the  $\hat{n}_c$  direction. Now, the simulation and desired angular momentum vectors can be expressed as

$$\vec{h}_S = I_n(\omega_1) \cdot \hat{n} + I_T(\omega_2) \cdot \hat{l} + I_T(\omega_3) \cdot \hat{m} \quad (13)$$

$$\vec{h}_c = I_n(\omega_{nc}) \cdot \hat{n}_c + I_T \cdot (\omega_o \cdot (I_{3 \times 3} - \hat{n}_c \cdot \hat{n}_c) \cdot \hat{o} + {}^L\vec{\omega}_B^*) \quad (14)$$

where  $\omega_1, \omega_2$  and  $\omega_3$  are the B-frame components of  ${}^A\vec{\omega}_C$ , and  $\omega_{nc}$  is the desired inertial sail spin given by

$$\omega_{nc} = \hat{n}_c \cdot {}^A\vec{\omega}_C = \hat{n}_c \cdot ({}^A\vec{\omega}_L + {}^L\vec{\omega}_B^* + {}^B\vec{\omega}_C) = \hat{n}_c \cdot {}^A\vec{\omega}_L = \hat{n}_c \cdot \omega_o \hat{o} \quad (15)$$

because  $\hat{n}_c \cdot {}^L\vec{\omega}_B^* = 0$  and choosing  ${}^B\vec{\omega}_C = 0$  for no sail spin rate relative to the L-frame for a non-spinning sail. The angular momentum error is then found to be

$$\Delta^A\vec{h}_C = \vec{h}_S - \vec{h}_c$$

$$\Delta^A\vec{h}_C = \underbrace{I_n\omega_1\hat{n} - I_n\omega_{nc}\hat{n}_c + I_T \cdot \omega_o \cdot ((I_{3 \times 3} - \hat{n} \cdot \hat{n}) \cdot \hat{o} - (I_{3 \times 3} - \hat{n}_c \cdot \hat{n}_c) \cdot \hat{o})}_{\Delta n\_term} + \underbrace{[I_T \cdot ({}^L\vec{\omega}_B - {}^L\vec{\omega}_B^*)]}_{\Delta \omega\_term} \quad (16)$$

where the error term is decomposed into and expressed as a function of sail normal angular position and sail normal angular velocity components. In order to determine a control torque  $\tau_{control}$  that reduces the angular momentum error, a Lyapunov stability approach will be used. First, a Lyapunov function candidate is defined.

$$V = \frac{1}{2} (\vec{h}_s - \vec{h}_c)^T (\vec{h}_s - \vec{h}_c) \quad (17)$$

From Eq. 17, the function  $V$  is positive definite with respect to angular momentum error. The behavior of the derivative of  $V$  can then be used to infer the behavior of the angular momentum error.

$$\begin{aligned} \frac{dV}{dt} &= \frac{{}^L d(\vec{h}_s - \vec{h}_c)^T}{dt} \cdot (\vec{h}_s - \vec{h}_c) = \left[ \frac{{}^A d(\vec{h}_s - \vec{h}_c)^T}{dt} - {}^A \omega_L \times (\vec{h}_s - \vec{h}_c) \right] \cdot (\vec{h}_s - \vec{h}_c) \\ &= \frac{{}^A d(\vec{h}_s - \vec{h}_c)^T}{dt} \cdot (\vec{h}_s - \vec{h}_c) \end{aligned} \quad (18)$$

Because the inertial derivative of angular momentum yields torque, the derivative of  $V$  can also be expressed as

$$\begin{aligned} \frac{dV}{dt} &= (\tau_s - \tau_c)^T \cdot (\vec{h}_s - \vec{h}_c) \\ \tau_s &= \tau_{se} + \tau_{control} \\ \tau_c &= \tau_{ce} + \tau_{stay\_cone} \end{aligned} \quad (19)$$

where  $\tau_s$  and  $\tau_c$  are total torques of the actual (simulation) and desired coning trajectory,  $\tau_{se}$  and  $\tau_{ce}$  are environmental torques of the simulation and coning trajectory,  $\tau_{stay\_cone}$  and  $\tau_{control}$  are the additional torques required to stay on the desired cone and the control torque applied in the simulation, respectively. The derivative of  $V$  becomes

$$\begin{aligned} \frac{dV}{dt} &= (\tau_{control} - \tau_{stay\_cone} + \delta\tau_e)^T \cdot (\vec{h}_s - \vec{h}_c) \\ \delta\tau_e &= \tau_{se} - \tau_{ce} \end{aligned} \quad (20)$$

In order to ensure that the derivative of  $V$  remains negative definite with respect to the angular momentum,  $\tau_{control}$  should be chosen as

$$\tau_{control} = -k_{control} \cdot (\vec{h}_s - \vec{h}_c) + \tau_{stay\_cone} - \delta\tau_e \quad (21)$$

which enables the derivative of  $V$  to be negative definite, as desired.

$$\frac{dV}{dt} = -k_{control} (\vec{h}_s - \vec{h}_c)^T \cdot (\vec{h}_s - \vec{h}_c) \quad (22)$$

The stability analysis proves that  $\Delta^A \vec{h}_c$  decays to zero [9] and thus the control law enables  $\vec{h}_s$  to track  $\vec{h}_c$ , for any positive control gain,  $k_{control}$ .

Unfortunately, from examining the decomposed components within the angular momentum error (Eq. 16), the Lyapunov function is not positive definite with respect to the sail normal because  $V$  can be zero even when sail normal is not (a combination of non-zero sail normal angular position error and velocity error can enable  $V$  to become zero). Thus, whether the sail normal error ( $\Delta \hat{n} = \hat{n} - \hat{n}_c$ ) decays to zero has not been proven. Since the angular momentum error is a function of sail normal angular position (Eq. 16), the control law reducing  $\Delta^A \vec{h}_c$  is implemented anyway (below) with the hope that  $\Delta^A \vec{h}_c \rightarrow 0$  can cause  $\Delta \hat{n} \rightarrow 0$  and enable  $\hat{n}$  to track the desired  $\hat{n}_c$  on the coning trajectory.

The environmental torques act on the sail based on its attitude, and these attitudes differ in the simulation and on the desired coning trajectory, unless the simulation trajectory exactly matches the desired coning motion. Since the application of control torque  $\tau_{control}$  is intended to enable  $\Delta\vec{h} \rightarrow 0$ , and that may cause simulation sail attitude,  $\hat{n} \rightarrow$  desired cone sail attitude,  $\hat{n}_c$ , it may be reasonable to assume that  $\delta\tau_e$  is small. In this case

$$\begin{aligned}\frac{dV}{dt} &= (\tau_{control} - \tau_{stay\_cone})^T \cdot (\vec{h}_S - \vec{h}_C) \\ \tau_{control} &= -k_{control} \cdot (\vec{h}_S - \vec{h}_C) + \tau_{stay\_cone}\end{aligned}\quad (23)$$

The  $\tau_{stay\_cone}$  can be given by

$$\tau_{stay\_cone} = \tau_c - \tau_{ce} \quad (24)$$

where  $\tau_c$  is the torque required to trace the desired cone, which is rather complicated to calculate on-line (inertial derivative of the desired angular momentum, Eq. 14). The environmental torques on the desired cone,  $\tau_{ce}$  involve many estimates of environmental factors and thus their analytical predictions can become inaccurate. If possible, such calculations (variables involving many unknowns) on a small sailcraft should be avoided. They can be avoided with the idea that in  $\tau_{control}$ ,  $k_{control}$  is a user-defined constant term and can be chosen large enough such that its term in Eq. 23 dominates the effect of  $\tau_{stay\_cone}$ . With these simplifications, the Lyapunov function and control torque are approximated by

$$\begin{aligned}\frac{dV}{dt} &= (\tau_{control})^T \cdot (\vec{h}_S - \vec{h}_C) \\ \tau_{control} &= -k_{control} (\vec{h}_S - \vec{h}_C)\end{aligned}\quad (25)$$

#### 4. Results

The sail dynamics under the influence of environmental torques are presented for a non-spinning sail. The result for the equilibrium point,  $[\beta = 35^\circ, \phi = 0^\circ]$  is given. This equilibrium point is selected because it induces the largest orbital effects [6]. The control method performance in tracing the desired cone at orbit rate is examined. The robustness of the control method is tested by adding initial condition errors to the sail angular position (these simulate errors in the sail attitude that emerge from disturbances) and using larger coning cones (greater orbital effects can be induced with cones larger than  $1^\circ$ ). The control method is designed to reduce the angular momentum error. The Lyapunov function indicates the performance of the control method for reducing this error.

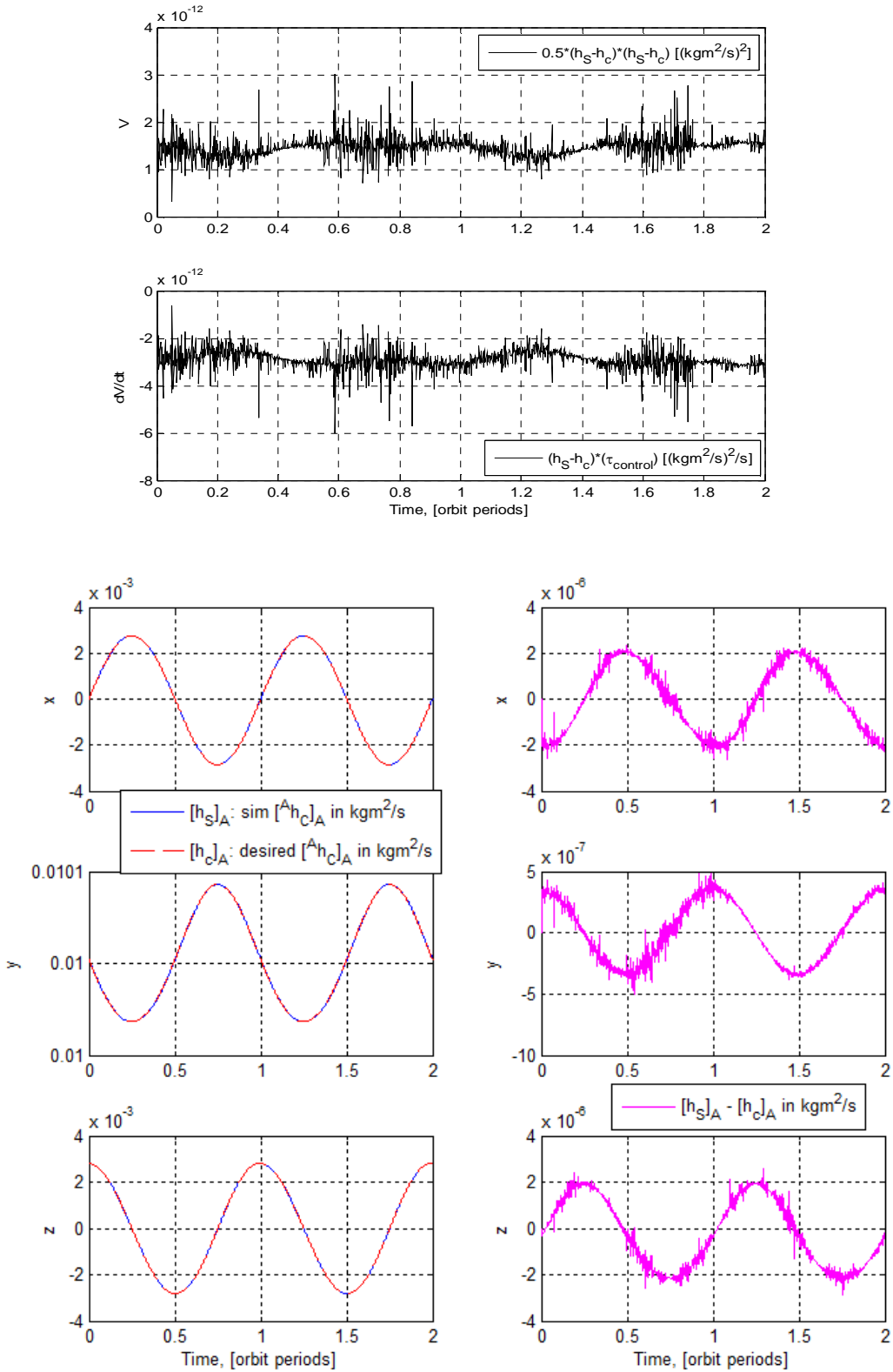


**Figure 15. Lyapunov Function, Its Approximated Derivative and A-frame Angular Momentum Components for Coning Trajectory having Half Cone Angle,  $\delta=1^\circ$  about a Nominal Sail Normal of  $\beta_0=35^\circ$ ,  $\Phi_0=0^\circ$**

The Lyapunov function  $V$  in Fig. 15, and thus the angular momentum error magnitude, is significantly lower than the absolute sailcraft angular momentum ( $\sim 10^3$  times lower). This indicates that the control method is successful in reducing the angular momentum error. On the other hand, even though the (approximate) derivative of  $V$  is always negative, the function  $V$  does not monotonically decrease. The derivative of  $V$  was approximated from

$$\frac{dV}{dt} = (\tau_{control} - \tau_{stay\_cone} + \delta\tau_e)^T \cdot (\vec{h}_S - \vec{h}_C) \text{ to } \frac{dV}{dt} = (\tau_{control})^T \cdot (\vec{h}_S - \vec{h}_C)$$

with simplifying assumptions eliminating  $\tau_{stay\_cone}$  and  $\delta\tau_e$ , as discussed earlier. In order to understand the incompatible behavior between  $V$  and its approximated derivative, the individual torque components in the non-approximated derivative are examined in Figure 16.

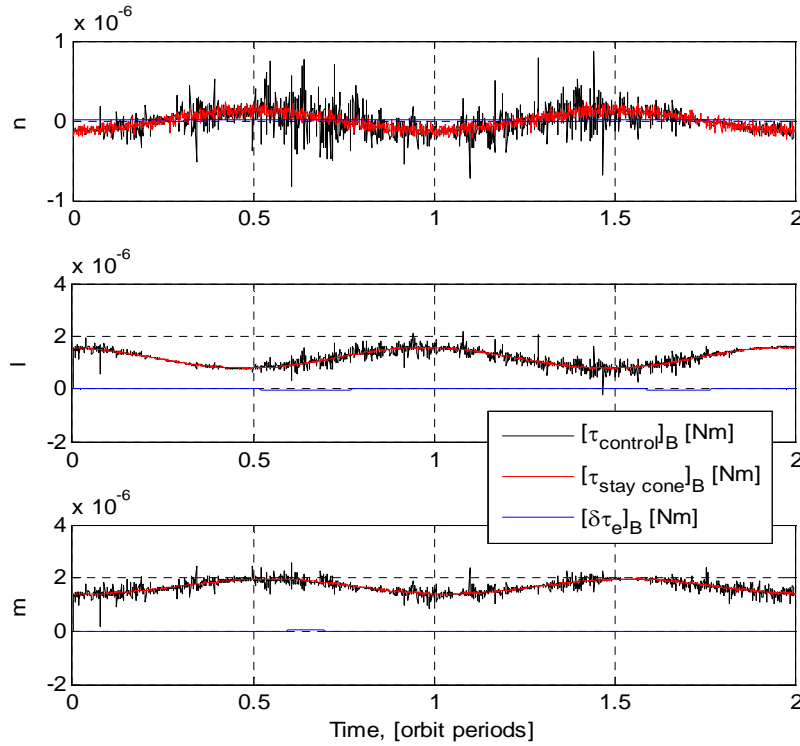


**Figure 16. Torques of the System in the B-frame**

The  $\tau_{control}$  is approximated using  $-k_{control}(\vec{h}_S - \vec{h}_C)$ . The magnitude is on the order of  $10^{-6}$  Nm, which is reasonably sized for a small sailcraft. For a similar 3 kg and  $40 \text{ m}^2$  solar sail, magnetic control was used to enable inertial coning of the sail normal at orbit rate and predicted maximum control torques on the order of  $10^{-5}$  Nm [10]. In Figure 16, the  $\delta\tau_e$  torque is  $\sim 10^3$  times lower in magnitude than  $\tau_{control}$  and  $\tau_{stay\_cone}$ , justifying the assumption of elimination  $\delta\tau_e$  from Eq. 23 ( $\delta\tau_e$  is negligible as compared with  $\tau_{control}$  and  $\tau_{stay\_cone}$ ). Note, however, that the  $\tau_{stay\_cone}$  torque is nearly identical (except for numerical noise) to the  $\tau_{control}$ . The  $\tau_{stay\_cone}$  is determined numerically by calculating the total torque  $\tau_c$  required for precessing the angular momentum on the desired cone and deducting the environmental torques,  $\tau_{ce}$  from  $\tau_c$  (Eqs. 24 and 26). The total torque on

the desired cone,  $\tau_c$  is the inertial derivative of the desired angular momentum,  $\dot{\vec{h}}_c$ . A numerical solution for  $\tau_c$  can be obtained via a finite difference

$$\tau_c = \frac{\vec{h}_{c2} - \vec{h}_{c1}}{t_2 - t_1} = \frac{\Delta \vec{h}_c}{\Delta t} \quad (26)$$

where  $\Delta \vec{h}_c$  is the change in desired angular momentum over a period of time,  $\Delta t$ . The  $\vec{h}_{c1}$  and  $\vec{h}_{c2}$  are calculated at times  $t$  and  $t + \Delta t$  via Eq. 14. The magnitude of  $\Delta t$  is decreased enough (with machine limitations) to approximate  $\Delta t \rightarrow 0$ . When the non-approximated derivative of  $V$  is used that includes the effects of  $\tau_{stay\_cone}$  and  $\tau_{ce}$ , the Lyapunov function and its derivative correspond to each other.

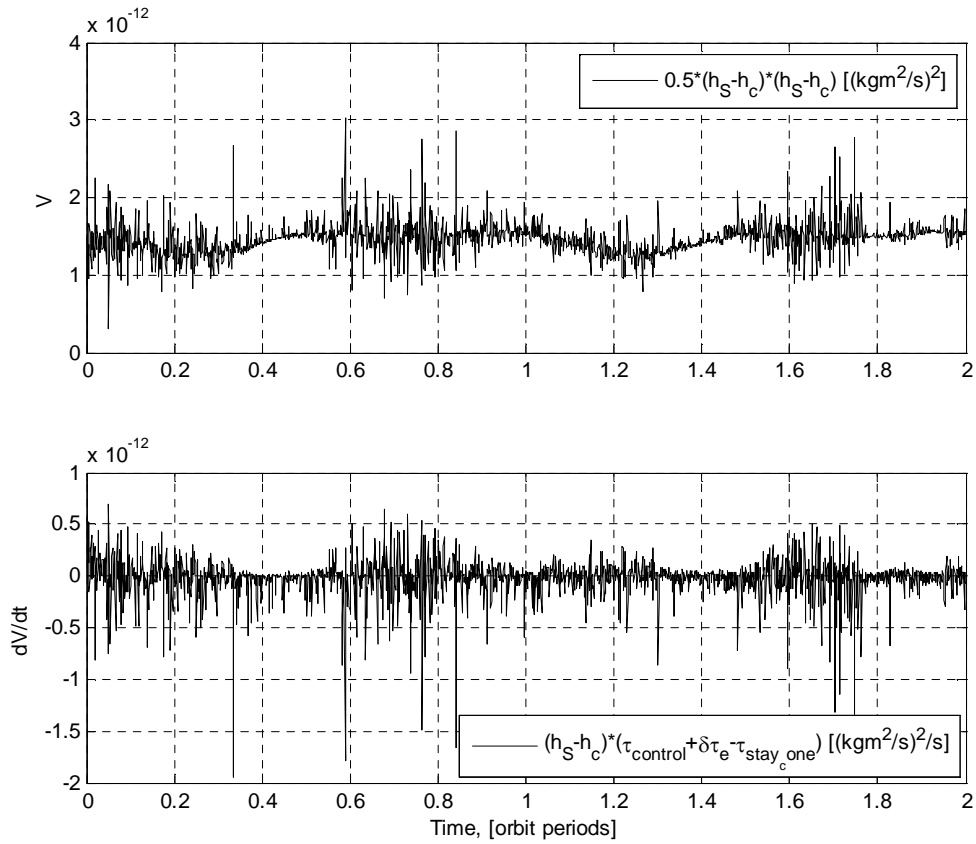


**Figure 17. Lyapunov Function and Its Derivative**

The derivative is no longer always negative explaining why  $V$  does not decrease. Even though  $V$  does not decrease, the oscillations of  $V$  are bounded. This indicates that the momentum errors within the system remain bounded and do not grow with time. Since  $V$  is a measure of the angular momentum error, the control method thus enables the sail angular momentum to trace the desired with some small, bounded error.

In Figure 16, the  $\tau_{stay\_cone}$  torque is essentially identical to the control torque,  $\tau_{control}$ . Observe that the actual torque on the system from the simulation,  $\tau_S$  and total torque required to stay on the desired cone,  $\tau_c$  are given by

$$\begin{aligned}\tau_S &= \tau_{actual/sim} = \tau_{se} + \tau_{control} \\ \tau_c &= \tau_{required} = \tau_{ce} + \tau_{stay\_cone}\end{aligned}\quad (27)$$

When  $\delta\tau_e$  is negligible, the environmental torques  $\tau_{se}$  and  $\tau_{ce}$  can be expressed as

$$\delta\tau_e = \tau_{se} - \tau_{ce} \rightarrow 0 \Rightarrow \tau_{se} = \tau_{ce} = \tau_e \quad (28)$$

from which the total system and desired cone torques become

$$\begin{aligned}\tau_S &= \tau_{actual/sim} = \tau_e + \tau_{control} \\ \tau_c &= \tau_{required} = \tau_e + \tau_{stay\_cone}\end{aligned}\quad (29)$$

From these equations, in order to trace the desired cone and induce the required angular momentum precession rate, we *must* have the total simulation torque,  $\tau_S \rightarrow$  the desired cone torque,  $\tau_c$ . This explains the behavior in Figure 16, where  $\tau_{control}$  is found to be identical to  $\tau_{stay\_cone}$ .

The corresponding behavior for the sail normal is shown in Figure 18.

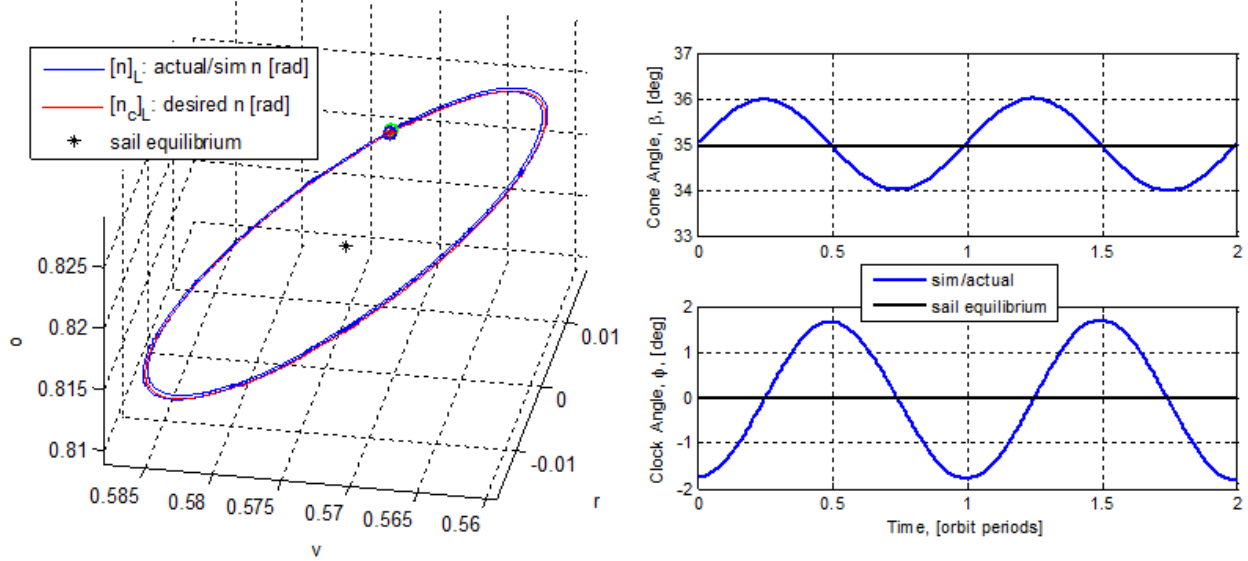


**Figure 18. Sail Angular Positions for Coning Trajectory having Half Cone Angle,  $\delta=1^\circ$  about a Nominal Sail Normal of  $\beta_0=35^\circ$ ,  $\Phi_0=0^\circ$  in the L-frame**

The three-dimensional plot indicates that the control method enables the simulation sail normal  $\hat{n}$  to trace the desired circular cone. The simulation and desired trajectories in this case begin at the same initial conditions. In the cone and clock angles plot, both  $\beta$  and  $\phi$  complete one cycle in one orbital period and repeat the same pattern in the next orbital period. Thus, the control method also enables orbit rate coning. The errors in the individual components of sail normal in the coning tracing are shown in Figure 19.

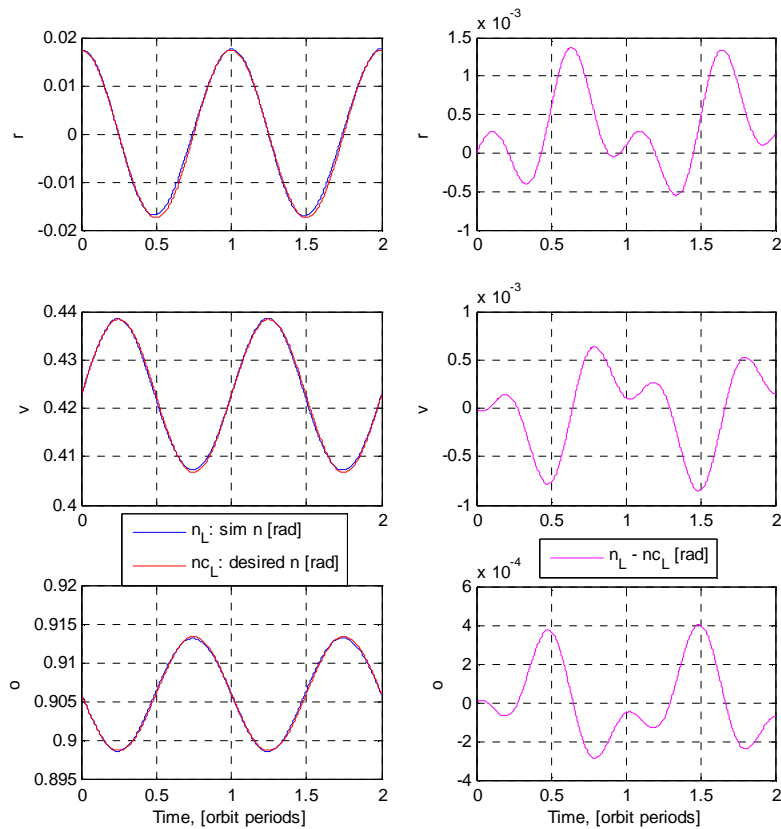


**Figure 19. Individual L-frame Components of Simulated and Desired Sail Normal with Errors**

As the cone is traced, Figure 19 shows that the error magnitudes of the  $\hat{r}$ ,  $\hat{v}$  and  $\hat{o}$  sail normal components oscillate. Even though there are errors in the coning tracing, they appear to be bounded. In addition, the error magnitudes are significantly lower than the absolute component magnitudes ( $10^1$ - $10^3$  times lower). McMahon, et. al. assert that the shape of the coning need not be accurate as long as orbit rate coning is achieved in order to yield the orbital effects [6]. Thus, slight deviations from the circular coning are not expected to have significant deviations in the averaged orbital effects induced over an entire orbit.

A sensitivity analysis is performed where the control gain,  $k_{control}$  is varied to study the maximum angular position error between the simulated and desired sail normal. The angular position error definition is illustrated in Figure 20.

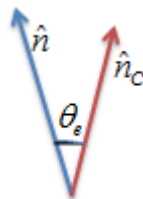


**Figure 20. Angular Position Error**

The angular difference between the desired and simulated sail normal is defined as the angular position error. The  $k_{control}$  was varied over a range of 0-2 and the variation in maximum angular error (over one orbital period) was studied. In order to understand the results, the angular error between the simulated and desired angular momentum is also shown.

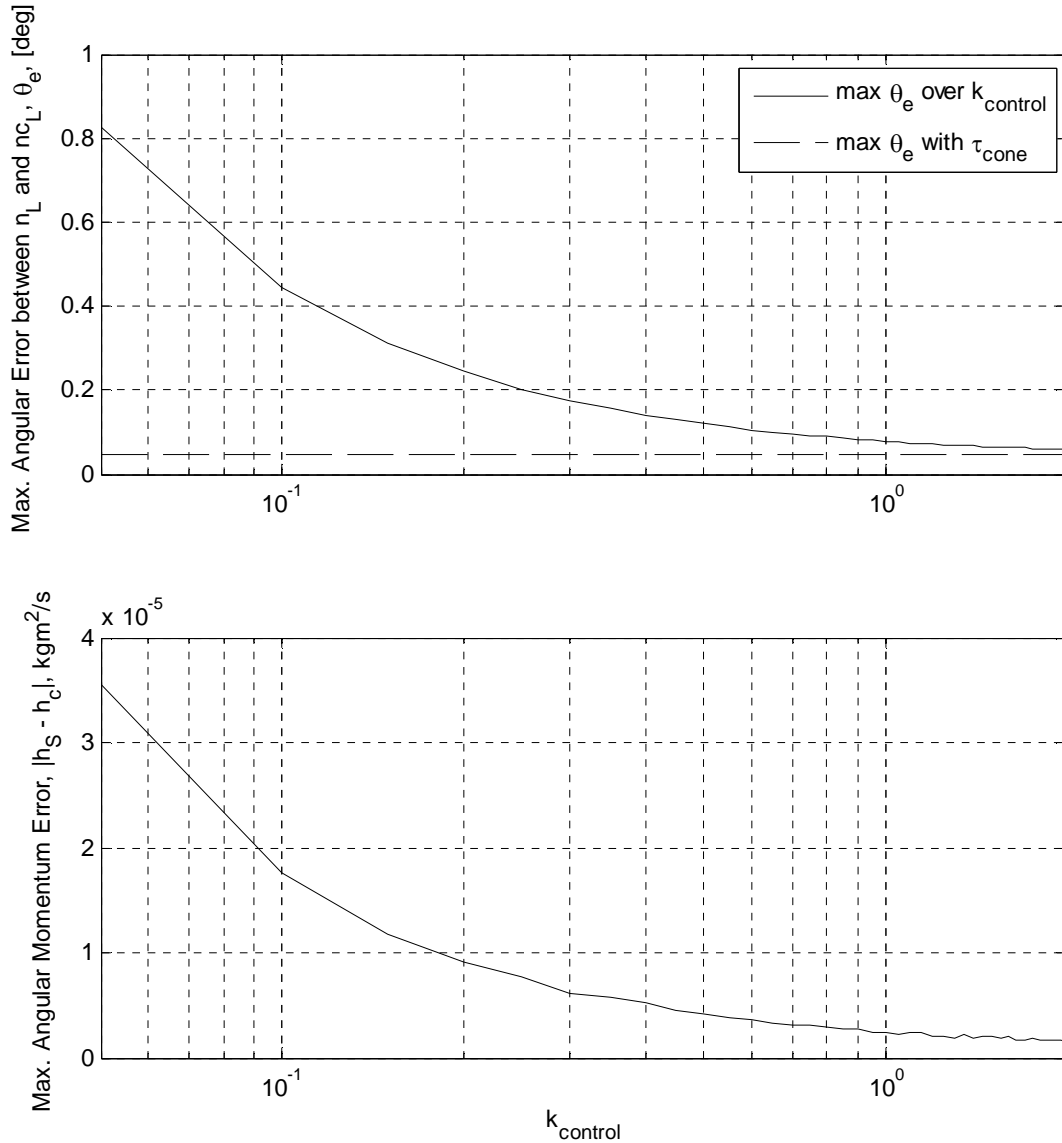


**Figure 21. Sensitivity Analysis of Maximum Angular Position and Momentum Error (for One Orbital Period) to variations in  $k_{control}$**

The angular position error,  $\theta_e$  decreases more rapidly with steadily increasing  $k_{control}$ . As the magnitude of  $k_{control}$  increases, the decrease in  $\theta_e$  becomes less rapid, until the limiting  $\theta_e$  of  $0.05^\circ$  is reached (indicated by the dashed line). Smaller  $k_{control}$  magnitudes result in smaller control torque magnitudes at each time step. With smaller control torque magnitudes, the simulated angular momentum is not corrected to trace the desired angular momentum as rapidly. This means that

the angular momentum error is larger for smaller  $k_{control}$  magnitudes. As  $k_{control}$  increases, the angular momentum is corrected more rapidly to trace the desired. This results in a smaller error. The angular momentum error decays rapidly with increasing  $k_{control}$ . Since the angular position error is a function of angular momentum error, the  $\theta_e$  also decays in a similar fashion. Ideally, the error should decay to zero as increasing control torque will enable the simulation to trace the desired exactly. However, the  $\theta_e$  decays to a limiting value and not zero. This is because  $\theta_e$  is calculated using the simulated trajectory and desired *analytical* trajectory, whereas the control torque is a function of simulated trajectory and desired *numerical* trajectory. This means that the simulated trajectory traces the desired *numerical* trajectory and not *analytical*. The difference between *analytical* and *numerical* desired trajectories is shown in Figure 22.

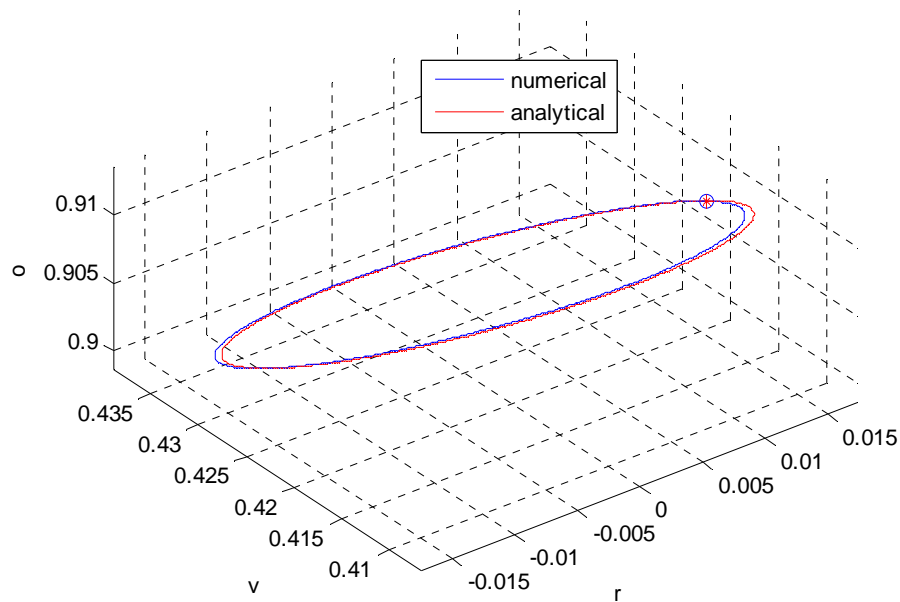


**Figure 22. Numerical and Analytical Desired Coning Trajectories having Half Cone Angle,  $\delta=1^\circ$  about a Nominal Sail Normal of  $\beta_0=35^\circ$ ,  $\Phi_0=0^\circ$  (One Orbital Period)**

The total torque on a coning trajectory (half cone angle,  $\delta = 1^\circ$ ) for a given nominal  $\beta_0 = 35^\circ$  and  $\phi_0 = 0^\circ$  is calculated using Eq. 26 (calculate  $\tau_c$ ). This torque was applied in the simulation to yield the *numerical* coning trajectory. Differences exist because the instantaneous derivative of desired angular momentum is not available ( $\tau_c$  is calculated numerically). The maximum angular position error between the *analytical* and *numerical* coning trajectories was found to be  $0.05^\circ$ . Hence, the  $\theta_e$  in Figure 21 decays to the numerical desired trajectory and reaches a limiting value of  $0.05^\circ$  (same as the maximum angular position error between the *analytical* and *numerical* coning trajectories).

The performance of the control method with the exact initial conditions has been presented so far. Practically, internal/external disturbances on the sailcraft causes initial condition errors with the sail attitude. Thus, the performance with initial condition errors should also be analyzed. Figure 23 illustrates how initial condition errors are added to the system.

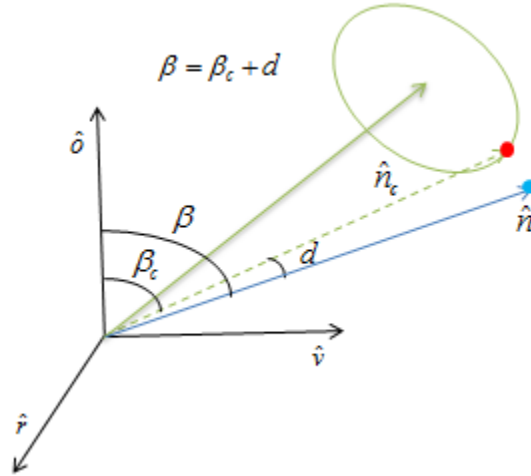


**Figure 23. Initial Condition Error**

The red dot represents the exact initial conditions for the system. The initial condition error is obtained by adding an angular deviation  $d$  such that the initial angular position (and hence initial angular velocity) contains errors with respect to the desired coning trajectory. The control method performance for  $1^\circ$  and  $10^\circ$  deviations follows.

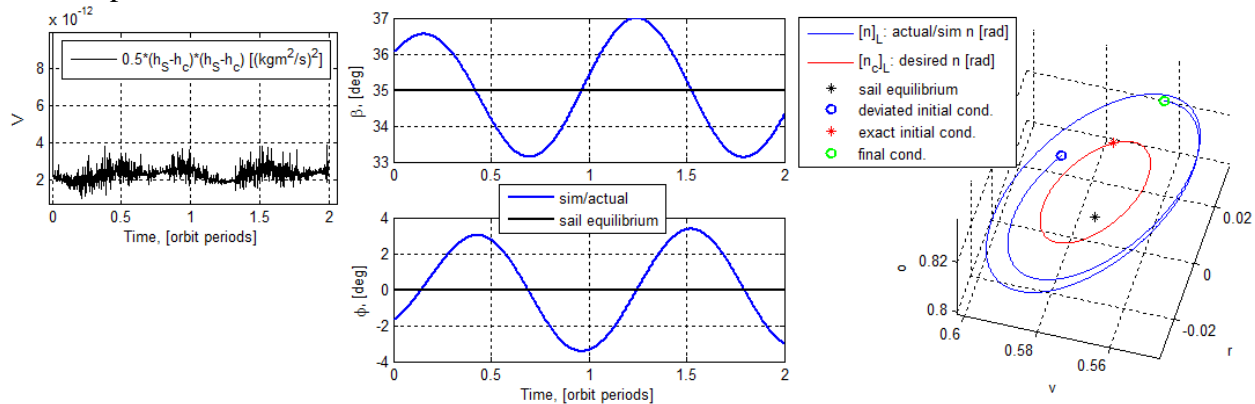


**Figure 24. Control Method Performance in Tracking Desired Angular Momentum and Sail Normal with Initial Condition Error of  $1^\circ$  ( $d=1^\circ$ ), Zero Sail Spin**

The Lyapunov function decreases to the levels as with no initial condition errors. This means that the control method is able to track the desired angular momentum vector even with the initial condition error. The sail normal motion is coning about the sail equilibrium point, however the desired normal is not traced as well as with no initial condition errors. The rate of coning has also deviated slightly from orbit rate. The Lyapunov function levels drop to the expected levels after one time step. This is clearly evident in the sail angular momentum vector motion shown in Figure 25.

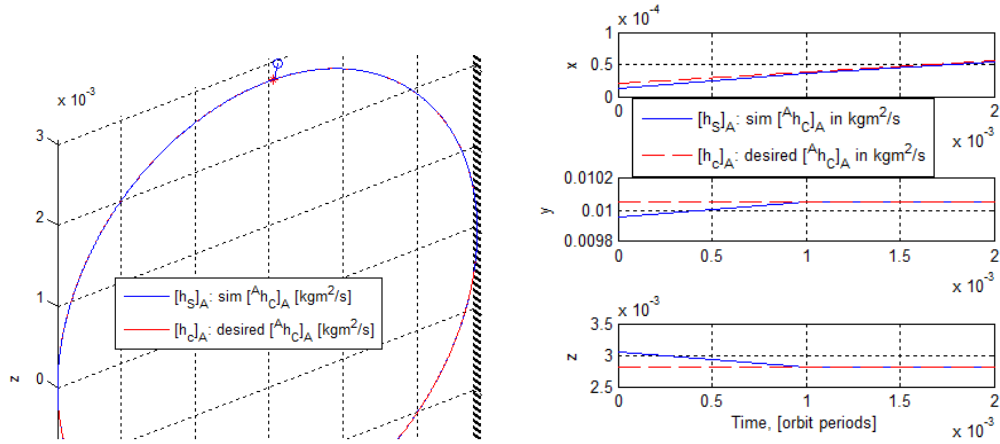


**Figure 25. Simulated and Desired Angular Momentum for Coning Trajectory with Initial Condition Error,  $d=1^\circ$ ,  $k_{control}=1$**

As expected, as the control authority is decreased ( $k_{control} = 0.1$ ), the simulation angular momentum tracks the desired cone more gradually (see Figure 26).

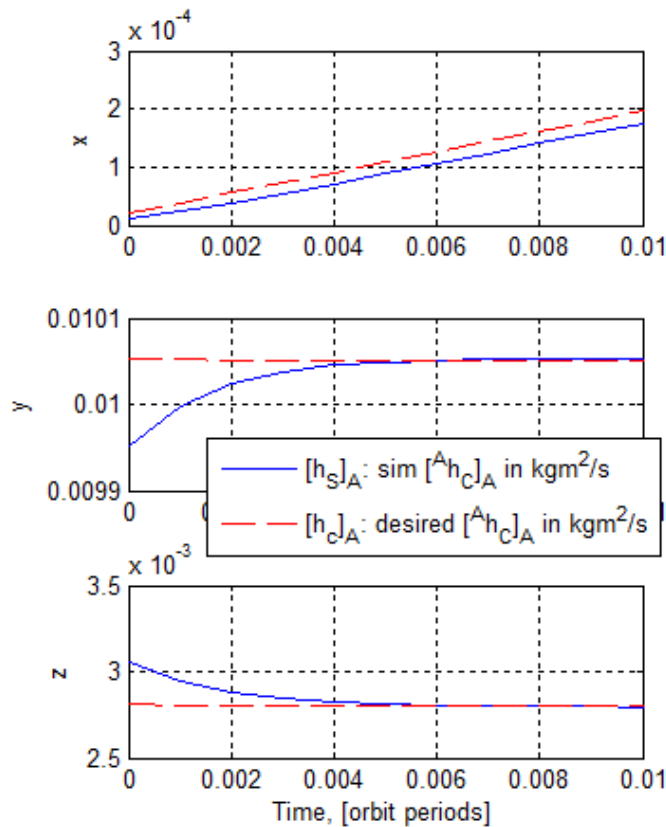


**Figure 26. Simulated and Desired Angular Momentum for Coning Trajectory with Initial Condition Error,  $d=1^\circ$ ,  $k_{control}=0.1$**

With decreased control authority, the control torque application is reduced which enables the sail angular momentum to track the desired gradually instead of after one time step. This behavior is preferable in a small sailcraft to avoid any abrupt changes to the attitude that can damage the sail.

The result with a larger initial condition error of  $10^\circ$  is presented in Figure 27.

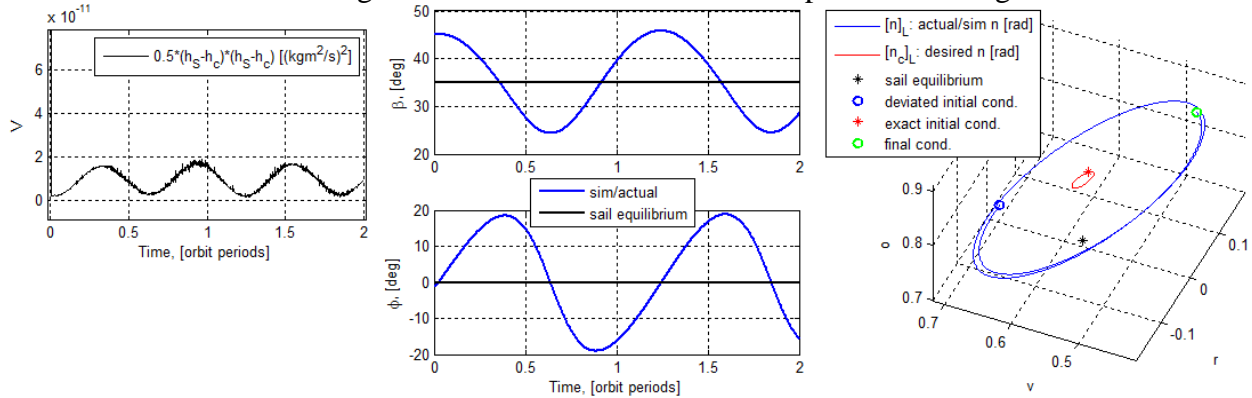


**Figure 27. Control Method Performance in Tracking Desired Angular Momentum and Sail Normal with Initial Condition Error of  $10^\circ$  ( $d=10^\circ$ ), Zero Sail Spin**

The control method performance in tracing the desired angular momentum has deteriorated slightly, which is indicated by the Lyapunov function magnitude increase as compared with the  $1^\circ$  deviation case ( $\sim 10$  times increase). However, there is significant deterioration in tracing the desired sail normal as compared with the  $1^\circ$  error case. The sail normal appears to trace a larger cone at a slightly different rate. This means that even though the control method performance did not deteriorate noticeably in tracing the desired angular momentum, the performance degraded significantly in tracing the desired sail normal.

The control method robustness is further examined by analyzing the results for tracing larger cones (larger half-cone angles). The results for  $5^\circ$  and  $60^\circ$  cones are presented below.

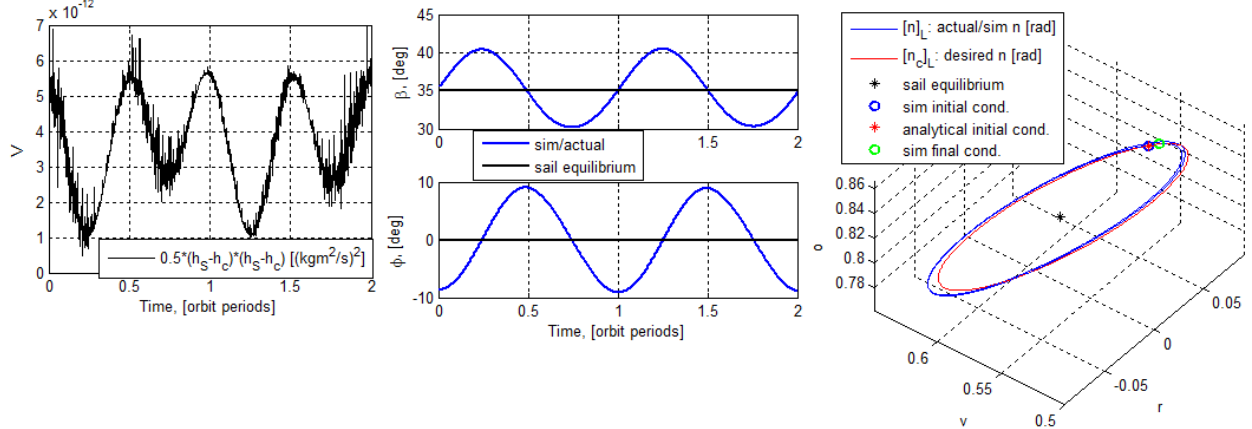


**Figure 28. Control Method Performance in Tracking Desired Angular Momentum and Sail Normal with  $5^\circ$  cone, Zero Sail Spin**

The errors from tracking the desired angular momentum are on the same order of magnitude as for the  $1^\circ$  cone (Lyapunov function level has the same order of magnitude). In addition, there are no significant deviations from orbit rate coning of the sail normal vector. The sail normal motion tracks the desired  $5^\circ$  circular cone with no significant differences as compared with the  $1^\circ$  cone case.

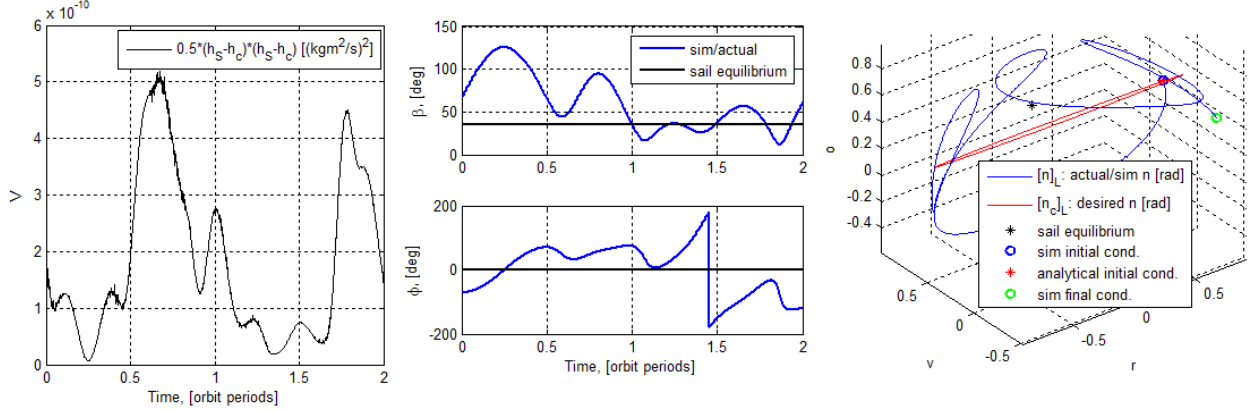


**Figure 29. Control Method Performance in Tracking Desired Angular Momentum and Sail Normal with 60° cone, Zero Sail Spin**

However, the control performance has deteriorated significantly for cones as large as 60°. The sail normal does not cone around the equilibrium point. The angular momentum tracking also has increased errors as compared with smaller cones ( $\sim 10^2$  times larger).

## 5. Conclusion

Sail attitude equilibria exist in the LVLH frame under the influence of gravity gradient, aerodynamic and solar torques. When the sail normal is precessed, the sail normal naturally cones about that equilibrium point. However, the sail normal coning has to follow a circular coning trajectory at orbit rate to induce the desired orbital effects. In this paper, a control method is developed that enables sail normal coning (circular cones) about the LVLH attitude equilibria at orbit rate. The control method is designed such that the sail angular momentum tracks a desired trajectory. The control method causes the sail angular momentum to track the desired angular momentum on the coning trajectory over an orbit and reduces the initial angular momentum error. Since angular momentum is a function of the sail angular position (sail normal), a reduction in angular momentum error is hoped to reduce the sail normal error between the actual and desired sail normal vectors on the coning trajectory. The performance of the angular momentum error reduction control method is analyzed using a case where the sail normal is tracking a 1° circular cone at orbit rate about an LVLH equilibrium point which induces the maximum orbital effects.

At this equilibrium, the control method allows the actual sail normal to trace the desired sail normal on the circular coning trajectory at orbit rate with an accuracy of 0.05°. The coning is at orbit rate (accurate coning rate), but there are errors in the shape of the coning (inaccurate circular coning). Even though there are errors in the circular cone tracing (10 to  $10^3$  times lower than the absolute sail attitude), they are bounded. In addition, past work asserts that the shape of coning need not be as accurate as long as orbit rate coning is achieved in order to attain the desired orbital effects. Thus, slight deviations from circular coning that cause these error magnitudes in the cone tracing are within the acceptable range. Studies are performed to analyze the control method performance when the sail normal position is deviated from the desired coning trajectory and while tracking larger cones. The performance of the control method deteriorates (deviated from orbit rate coning and had increased circular cone tracing errors) when the initial condition deviation was increased to 10° and cones became as large as 60°. In

summary, this control method functions well for tracking the desired angular position (sail normal) at the chosen LVLH equilibrium point, for small cones and small initial condition errors.

Past work analyzed orbit rate coning for circular coning trajectories in order to induce the desired orbital effects. The assumption for circular coning can be relaxed and induced orbital effects for non-circular cones can be studied. A non-circular cone alters the sail normal thrust vector direction relative to the sun differently. This produces different orbital changes whose usefulness can be analyzed. This could relieve the control method from the need to provide perfectly circular cone tracing and only concentrate on enabling orbit rate coning.

In this work, a flat, rigid sail model is used. A large, gossamer sail is not perfectly flat or rigid in space. This work can be further extended to include non-flat, non-rigid sail dynamics. Finally, the practical implementation of the control torque required to enable the orbit rate coning of the desired trajectory with the existing hardware can be studied (e.g. using reaction wheels, tip vanes, or sailcraft bus deflection).

## 6. References

- [1] Stough, R., Heaton, A. and Whorton, M., "Chasing a Comet with a Solar Sail," *Proc. of AAS/AIAA Space Flight Mechanics Conf.*, AAS 08-171.
- [2] Rizvi, F. and Lawrence, D. "Attitude Actuation Alternatives for Small Solar Sails," *Proc. of AAS Guidance and Control Conf.* AAS 09-083.
- [3] Macdonald, M., Hughes, G., McInnes, C., Lyngvi, A., Falkner, P. and Atzei, A., "GeoSail: An Elegant Solar Sail Demonstration Mission," *Journal of Spacecraft and Rockets*, Vol. 44, No. 4, pp. 784-795, 2007.
- [4] Lappas, V., Wie, B., McInnes, C., Tarabini, L., Gomes, L. and Wallace, K., "Microsolar Sails for Earth Magnetotail Monitoring," *Journal of Spacecraft and Rockets*, Vol. 44, No. 4, pp. 840-848, 2007.
- [5] Lawrence, D. and Whorton, M., "Solar Sail Dynamics and Coning Control in Circular Orbits," *Journal of Guidance, Control, and Dynamics*, Vol. 32, No. 3, 2009, pp. 974-985, 2009.
- [6] McMahon, J. and Lawrence, D. "Orbital Maneuvering with a Solar Sail Through the use of Natural Attitude Coning," *Proc. of AAS Astrodynamics Specialist Conf.* AAS 09-345.
- [7] Swartwout, M., "Earth Escape Using a Slowly Rotating, Doubly Reflective Sail," *Journal of Guidance, Control and Dynamics*, Vol. 28, No. 2, pp. 374-377, 2005.
- [8] Robertson, R., "Two Decades of Spacecraft Attitude Control," *Proc. of 18<sup>th</sup> AIAA Aerospace Sciences Meeting*, Huntsville, AL, Jan, 1978, AIAA 1978-7.
- [9] Schaub, H. and Junkins, J., *Analytical Mechanics of Space Systems (2<sup>nd</sup> Edition)*. Virginia: AIAA, Inc., 2009.

[10] Lawrence, D. and Whorton, M., "Coning Control of Solar Sails Using Magnetic Momentum Error Reduction," *Journal of Spacecraft and Rockets*, Vol. 46, No. 6, pp. 1298-1308, 2009.